



Article

Turbulence Structure and Dynamics Investigation of Turbulent Swirl Flow in Pipe Using High-Speed Stereo PIV Data

Djordje S. Čantrak * and Novica Z. Janković 

University of Belgrade, Faculty of Mechanical Engineering, Hydraulic Machinery and Energy Systems
Department, Kraljice Marije 16, 11120 Belgrade, Serbia; njankovic@mas.bg.ac.rs

* Correspondence: djcantrak@mas.bg.ac.rs

Abstract: Turbulent swirl flow, which exists in numerous turbomachinery systems, is the focus of this paper. It consumes a significant amount of energy, so it is a subject of investigation for many researchers. It is even more present in ventilation systems, as numerous axial fans are still installed without guide vanes. The experimental investigation of the turbulent swirl flow behind an axial fan in a pipe, installed in a test rig with a free inlet and ducted outlet, as defined in the international standard ISO 5801, is presented in this paper. Moreover, in this paper, the axially restricted case is studied. A designed axial fan generates a Rankine vortex with a complex structure, and research on the vortex turbulence structure and dynamics is presented. On the basis of the HSS PIV (high-speed stereo particle image velocimetry), measurement results are calculated using invariant maps. All states of turbulence anisotropy are thoroughly analyzed by applying the invariant theory on HSS PIV results. Vortex dynamics is observed on the basis of the total velocity minima positions and their repetitions. Both methods are correlated, and important conclusions regarding vortex behavior are deduced.



Citation: Čantrak, D.S.; Janković, N.Z. Turbulence Structure and Dynamics Investigation of Turbulent Swirl Flow in Pipe Using High-Speed Stereo PIV Data. *Energies* **2022**, *15*, 5417. <https://doi.org/10.3390/en15155417>

Academic Editors: Maria Grazia De Giorgi, Donato Fontanarosa and Antonio Ficarella

Received: 1 July 2022

Accepted: 24 July 2022

Published: 27 July 2022

Publisher's Note: MDPI stays neutral with regard to jurisdictional claims in published maps and institutional affiliations.



Copyright: © 2022 by the authors. Licensee MDPI, Basel, Switzerland. This article is an open access article distributed under the terms and conditions of the Creative Commons Attribution (CC BY) license (<https://creativecommons.org/licenses/by/4.0/>).

Keywords: turbulent swirl flow; axial fan; vortex dynamics; invariant maps; high-speed PIV

1. Introduction

Turbulent swirl flow, which exists in many technical and transportation systems, in some bioengineering applications, in the atmosphere, and in nature in general, has attracted the attention of numerous researchers for decades. Experimental results are obtained for various cases of turbulent swirl flow, but general laws are still not established. Numerical models are developed on the basis of these experimental results, but only for specific cases. Researchers have made significant efforts regarding the complex research of the axial fans and their applications in various systems [1–4].

However, the focus of this paper is turbulent swirl flows in ventilation systems, but presented procedures could be employed in many technical applications. The influence of the ventilation channel geometry is minimized by introducing the circular pipe. Namely, today, in many applications turbomachines are still in-built without guide vanes, which minimize swirl flow. It was shown that friction factors are significantly higher with circulation than without it [5]. This generates greater hydraulic losses and changes the fan duty point if it is not designed in the proper way. The need for flow straighteners or guide vanes is also reported in [6,7]. Pump manufacturers are aware of this fact, and they strictly eliminate turbulent swirl flow in pumping systems, but it still exists in many ventilation systems. This paper presents a study of turbulent swirl flow in the pipe behind the axial fan impeller, which is a continuation of the well-established research at the University of Belgrade, Faculty of Mechanical Engineering (UB FME) [8].

The international standard ISO 5801:2007 “Industrial Fans-Performance Testing using Standardized Airways” recognizes various in-built strategies of fans in installations. This paper presents a category B installation with the fan ducted outlet. From the fan-design

point of view, this is an axially restricted case [9]. The optimal calculation of the impeller is based on taking into account all the in-built elements [10].

This case uses an axial impeller, which generates the Rankine vortex [10–15]. It is a combined vortex, with a solid body behaving in the central zone, while the free vortex is in the outer region. This free vortex core region, with constant circulation, was designed on purpose. In fact, it is a consequence of a design with a constant impeller head along the radius, and it neglects the pre-swirl occurrence [10–15]. This highly efficient design has twisted blades, which are more complex for production. The authors of [11] provided an overview of the turbulent swirl flow issues relevant for this investigation [11]. Here, experimental results are reported, obtained by use of the high-speed stereo particle image velocimetry (HSS PIV) measurement technique on the axial fan pressure side in the axially restricted installation, as presented in Figures 1 and 2.

This paper describes methods applied to these experimental results, where there is a coherent vortex structure. The first method is a set of statistical methods, which enables the observation of the vortex dynamics, i.e., the total velocity minima positions. This reveals energy consumption in ventilation systems with a developed swirl flow. The second method is the study of the flow anisotropy in anisotropy invariant maps, which is an efficient and comprehensive way to characterize turbulence flow tensor fields. In this paper, an approach to employ the invariant maps in turbulence research in turbomachinery on the basis of the HSS PIV experimental results is presented. The authors declare in paper [16]: “It is found that large degrees of turbulent anisotropy occurring in the region dominated by the oscillating vortex core”. So, this approach with anisotropy maps could quickly discover if the areas of isotropy occur, which would result in a non-oscillating vortex. Both methods, presented in this paper, confirm the above-mentioned conclusion from paper [16].

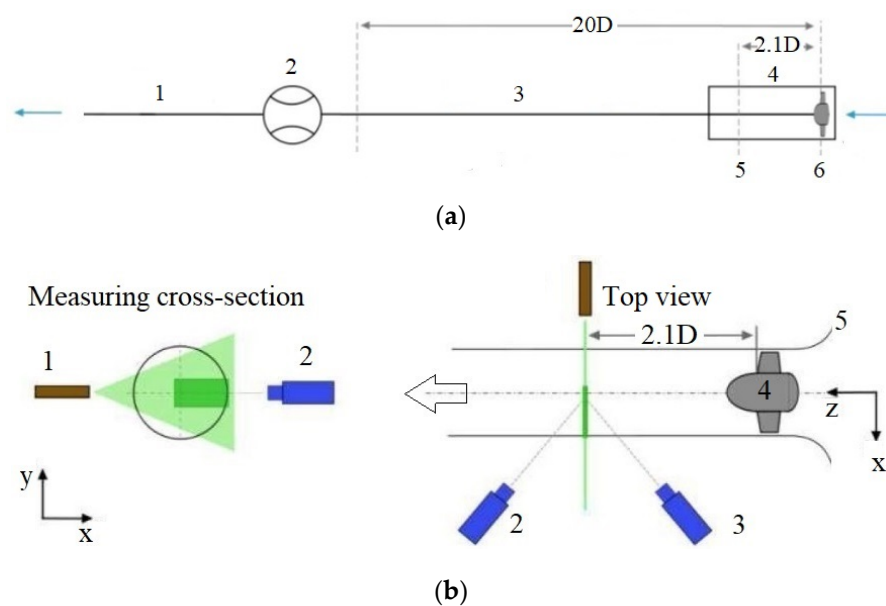


Figure 1. Test rig: (a) 1—flexible hose, 2—Venturi flow meter, 3—straight aluminum duct, 4—transparent pipe section, 5—measuring cross-section, and 6—axial fan impeller. (b) 1—Nd:YLF laser; 2 and 3—left and right PIV fast cameras, respectively; 4—axial fan impeller; and 5—profiled free bell-mouth intake.

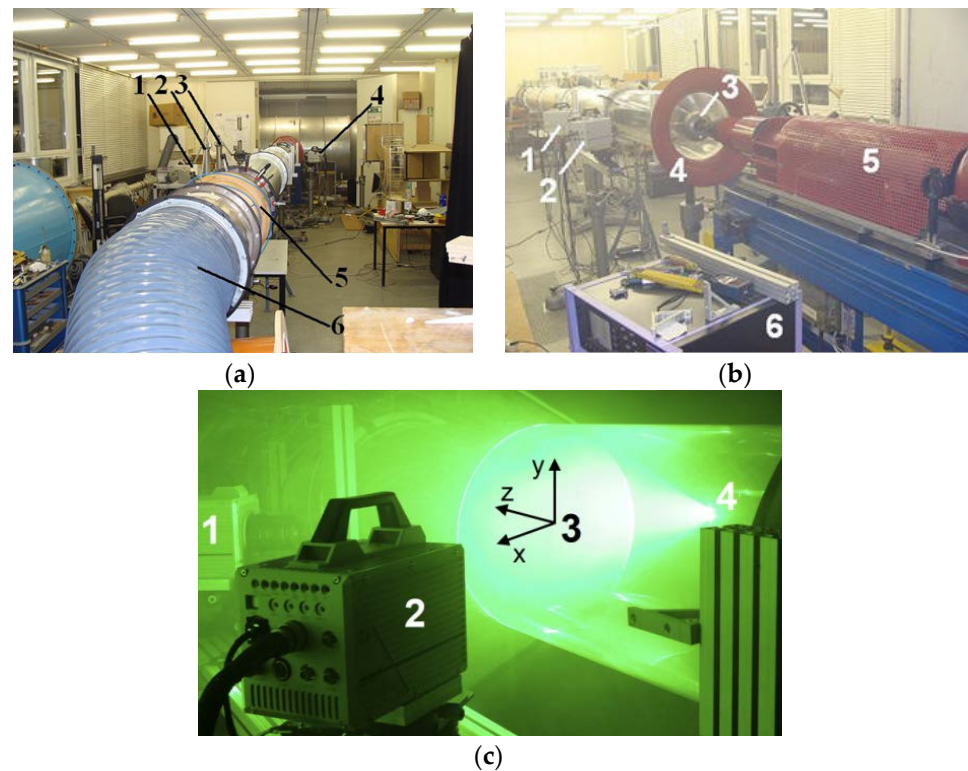


Figure 2. Test rig: (a) 1—Nd:YLF laser, 2 and 3—Betz micro-manometers, 4—PIV fast cameras, 5—Venturi flow meter, and 6—flexible hose; (b) 1—left PIV fast camera, 2—right PIV fast camera, 3—axial fan impeller, 4—profiled free bell-mouth intake, 5—DC motor with torque measurement, and 6—electric power meter; and (c) 1 and 2—fast cameras, 3—software coordinate system position in the measuring section, and 4—Nd:YLF laser.

2. Experimental Test Rig and Measurement Methods

The total length of experimental test rig was $22.67 \cdot D + \text{flexible hose}$, where an average inner diameter was $D = 0.404$ m (Figures 1 and 2). The flow direction is marked in Figure 1a.

The pipe non-transparent section was made of three aluminum pipes of 2 m each, with average diameter of 0.404 m. The sealing and leveling of the installation were also controlled. The motor group was heavy, positioned on four legs, and lay on the rubber. There were no fan vibrations. The axial fan impeller had a DC motor with torque measurement and an electric power meter (Figure 2b). The test rig was designed and constructed at the Institute of Fluid Machinery, Faculty of Mechanical Engineering, Karlsruhe Institute of Technology, Karlsruhe, Germany. The axial fan impeller and transparent pipe, 1.5 m long, with an attached profiled free bell-mouth intake, were made and transported from UB FME. The transparent pipe had a 5-mm wall thickness. This axial fan was also installed in the test rig with an added booster fan [12,13]. In this paper, the axial fan operated without the booster fan and had a different duty point and blade angle at the outer impeller diameter, which was positioned at angle 26° .

The axial fan impeller, designed to generate the Rankine vortex, had nine adjustable blades, an outer diameter 0.399 m, and a hub radius 0.1995 m. The axial fan impeller design is described, in more detail, in [10,11,14]. The fan inlet and outlet were designed as hydraulically smooth to ensure the absence of the pre-swirl flow, as well as to postpone the flow separation and decrease the vortex core region. The bell-mouth intake was positioned at the pipe inlet, as well as with the task to ensure the smooth test rig flow entrance (Figure 2b). In addition, the bearings were positioned at the distance from the pipe inlet to not obstruct the axial fan inlet side. The fan rotation speed was 500 rpm. The HSS PIV measurements were only performed in one section $z/D = 2.1$, where z was a coordinate

measured from the test rig inlet along the pipe axis measured from the blade trailing edge. The coordinate system orientation is presented in Figure 1b.

The flow was illuminated with a Darwin Duo-527-100-M dual oscillator. It is a single head and a diode-pumped Nd:YLF laser, with light arm and attached optics. It had an output light with a wavelength of 532 nm. Cameras were positioned in the stereo, Scheimpflug configuration, in a “forward scatter” mode (Figure 2c). Two fast cameras, model FASTCAM SA4, and Photron with CMOS sensors, were used. Canon EF 85mm f/1.8 USM lenses were used. The camera resolution at 4000 fps was 1024 pix x 1008 pix. Due to the camera memory limitation, only 5542 images were taken. The capturing time was approximately 1.4 s. The time distance between the two laser pulses (Δt) was chosen on the basis of the test pictures, where the particle displacement was observed. The time distance for this measurement was $\Delta t = 40 \mu\text{s}$. It was not possible to capture the velocity field along the whole radius at once. The flow was seeded with the thermal fog generated by the fog machine Antari Z3000II with liquid Eurolite Smoke Fluid “-X-Extrem A2”. The fog was naturally sucked in the installation by the axial fan. The post processing was realized using software PIVView ver. 3.3.2. The software coordinate system is specified in Figure 2c. The origin was on the pipe axis. Common methods of dewarping and disparity correction were applied, while the cross correlation had an interrogation area of 32×32 pixels and an overlap of 50%. The PIV uncertainty quantification has been studied and discussed in numerous papers [17]. Its quantification in swirling flow can be complex, as shown in [14] due to various flow zones. In paper [18], simultaneous laser Doppler anemometry (LDA) and PIV measurements were carried out in the test rig, where measurements presented in this paper were performed, with the same fan, but for a different Reynolds number. However, it was concluded in [18]: “The results show good correlation in time and magnitude. The mean offset, hence systematic error is in the range of around 0.5 m/s and independent of flow velocity and turbulence intensity”.

3. Flow Integral Parameters and Vortex Dynamics

The time average velocity fields (axial (U), radial (V), and circumferential (W)) are presented in Figure 3.

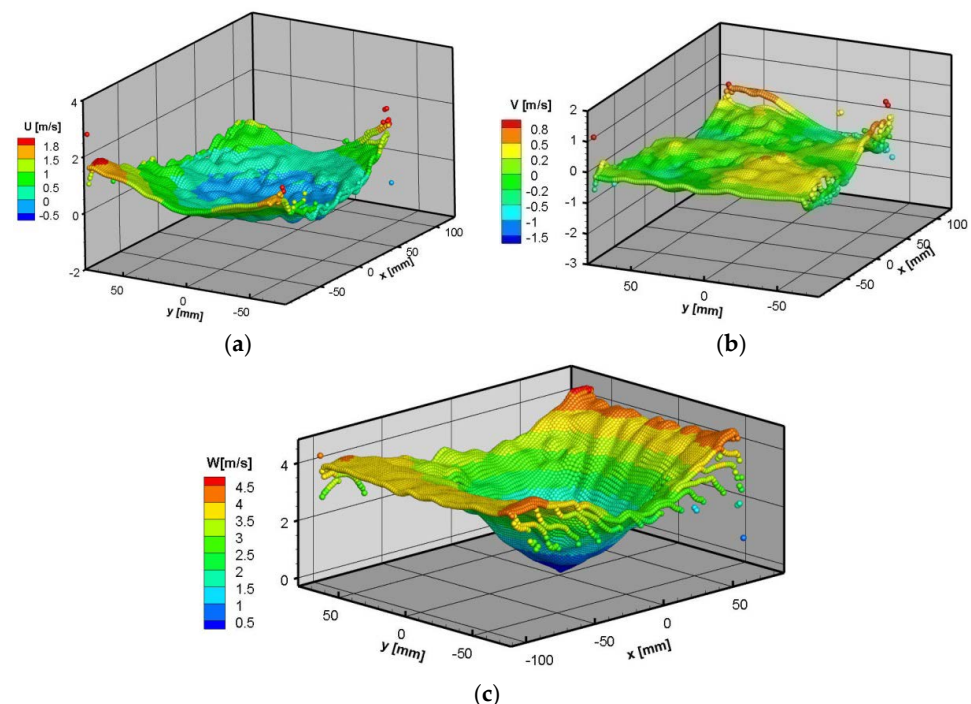


Figure 3. Measured time averaged velocities by HSS PIV in 1.4 s: (a) axial (U), (b) radial (V), and (c) circumferential (W) [14].

Axial velocity (U) has the lowest values in the vortex core region, where backflow occurs (Figure 3a). In the turbulent Rankine vortex, four zones could be distinguished. They are usually observed on the circumferential velocity profile [11–15]. The central region was observed, also known as the vortex core or forced vortex zone, characterized by a solid body, i.e., a linear distribution of the circumferential velocity; the shear layer region, characterized by the circumferential velocity maximum; and part of the sound flow region, where the circumferential velocity has a distribution of the potential swirl (Figure 3c). The rest of the sound flow region and the fourth, the boundary layer region, are not visible in this research. The vortex core, in the case of the observed type of the Rankine vortex, is defined in [12] as a region where the radial velocity (V) is low (Figure 3b), so the flow can be observed as quasi two-dimensional.

A Venturi flowmeter was installed in the test rig (Figure 1a, pos. 2 and Figure 2a, pos. 5), and a measured volume flow rate was $Q = 0.173 \text{ m}^3/\text{s}$. On the basis of this, the average velocity was calculated by the area $U_m = 4Q/D^2\pi = 1.34 \text{ m/s}$. The obtained Reynolds number was $Re = U_mD/\nu = 35,159$, where ν was the air kinematic viscosity.

Vortex dynamics are discussed on the basis of the observed total velocity fields and their minima. However, a set of the minimum velocity values $C_m = \{C_{m,i} | i \in N, i \leq n\}$, where the number of measurements is $n = 2771$, is determined on the basis of the measured velocity field statistical ensembles (U , V , and W). The set of values C_m corresponds to the statistical set of points $S = \{(x_{c_j}, y_{c_j}) | j \in N, j \leq n\}$, where the index c stands for the vortex center. A set S is a set of points $M_{c_j}(x_{c_j}, y_{c_j})$, i.e., the set of all points (x_{c_j}, y_{c_j}) that determines the j -th coordinates of the vortex center (x_c, y_c) in the certain arbitrary moment $0 \leq t \leq 1.4 \text{ s}$ (Figure 4). The time history of the velocity minima and their positions is analyzed in order to investigate the vortex oscillating phenomenon. An amplitude-frequency analysis of the random functions $x(t)$ and $y(t)$ (Figure 4) results in obvious peaks and frequency dependencies. Namely, Figure 4 shows both coordinates in time with period $T = 0.12 \text{ s}$, which corresponds to the frequency $f = 1/T = 8.33 \text{ Hz}$, i.e., the fan rotation number 500 rpm. This dependence between the frequency characteristics of the fan impeller and the vortex oscillation, generated by it, is important for engineering practice, energy consumption calculation, and fan design. Additionally, it is obvious that the absolute value of the $y \equiv y_c$ coordinate could achieve higher values than the $x \equiv x_c$ coordinate (Figure 4).

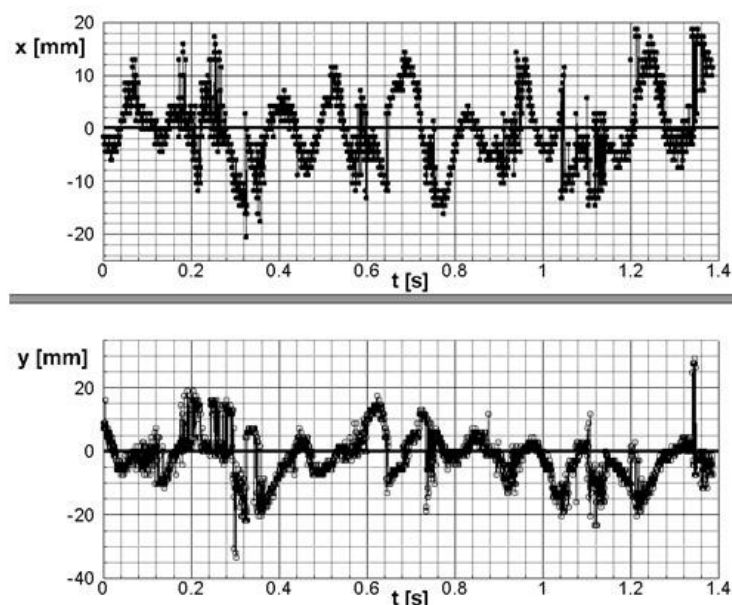


Figure 4. Time record of the total velocity minima in the measuring section (x_c (filled circles) and y_c (empty circles) are coordinates of the vortex center).

In any case, most of the minima are concentrated in the region $20 \text{ mm} \times 20 \text{ mm}$, which is inside of less than 5% of the inner pipe diameter. The ratio of surfaces of this region of the measurements section a_c and pipe A is $a_c/A = 0.0203$, which represents only 2%. It means that the vortex center stochastic movement is limited to a small region. A further statistical investigation of the correspondent sets of values C_m and S , the determined points $M_j(x_j, y_j)$ of the measurement section, revealed that the total velocity minimum occurs many times. This frequency of the existence of the total velocity minimum in a certain point is denoted with α . In this way, in the physical domain of n measurements ($n = 2771$), the geometry domain with the help of the set $G = \{M_j | j \in N, j \leq n_G\}$, where $n_G = 439$ points, is introduced. A set G is a subset of $F = \{M_i | i \in N, i \leq n\}$, i.e., $G \subseteq F$. For application, in this paper the chaotic vortex movement is analyzed by the use of the empirical probability distribution, i.e., the statistical distribution laws. Statistical sets C_m , S , and G are the basis for the numerical-empirical and geometry-graphical creation of the histogram of the absolute and relative frequencies of the total velocity minimum in certain measurement section domains, i.e., in certain sets of points in the measuring section.

The obtained results are analyzed in this paper by the physical-geometrical interpretation of the statistical distribution presented in the polygon of the relative frequency α (Figure 5). So, set ${}^\alpha G_k \subseteq G$ has k elements, i.e., has k points of the measuring section with the common characteristic that in each of them minimal velocities, and the same or various numerical values, occur α times, i.e., with the frequency α . This subset of the set G is mathematically defined with the expression ${}^\alpha G_k = \{M_j | j, \alpha \in N, j \leq k, k \leq n_G, \alpha \leq r, \alpha = \text{const.}\}$, where $\alpha = \alpha_k$, i.e., $k = k(\alpha)$ and $\alpha_{max} \equiv r = 48$ are empirical values.

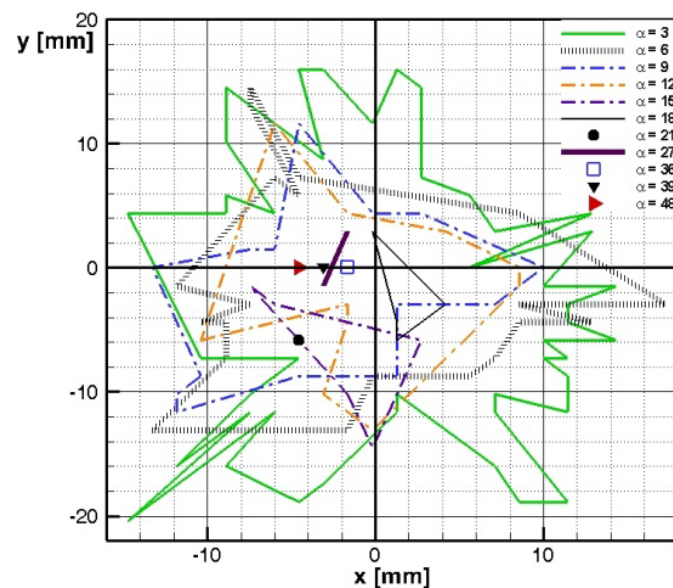


Figure 5. Polygon of frequencies (α) of certain vortex center positions in the measuring section.

In Figure 5, statistical data sets ${}^\alpha G_k$ for various frequencies $\alpha = 1, 2, \dots, r$ with the corresponding number of points $k(\alpha)$, which are not presented in the polygon, are geometrically presented. Moreover, the iso-frequency and closed or open lines $\alpha = \text{const.}$ are formed by all points of the measuring section xOy ($-20 \leq x \leq 20, -35 \leq y \leq 30$ [mm]), where the total velocity minima is with α frequency. The data set $\alpha = \{\alpha_i | \alpha_i = 1, 2, \dots, r, r = 48\}$ with $\alpha_i = \text{const}$ determines the empirical probability, i.e., the statistical frequency of the vortex center positions in the measuring section.

The highest frequency (α) is in the vicinity of the pipe axis (Figure 5). The highest number α is 48, while the highest percentage of points has seven repetitions. Figure 5 is formed starting from the number $\alpha = 3$ and continued with six, till the end with a step three. In some cases it happens, especially for higher α such as 21, 36, 39, and 48, that total velocity minima occurs in the same position, close to the pipe axis. The frequency $\alpha = 27$

has only two positions. So, it can be concluded that higher frequencies occur in the central zone, whereas unique points (frequency $\alpha = 1$ has 105 points, which are elements of the subset ${}^\alpha G_k = \{ {}^\alpha M_j | j \in N, j \leq 105, \alpha = 1 \}$ of the set G) and those with lower repetition rates occur in a wider area. The center of the vortex is approximately on the pipe axis. The zone of the turbulent vortex dynamics and its dynamics could be observed in this way. These developed and applied methods are significant for further statistical investigations of the vortex structure and the intermittency of vortex coherent structures in the core and shear layer of the investigated turbulent swirl flow behind the axial fan impeller.

4. Vorticity and Vortex Detection

The average vorticity field (Ω_z) is presented in Figure 6. It reveals the vortex structure, with the vortex core zone in the middle and ring zone of the highest vorticity, i.e., the shear layer region.

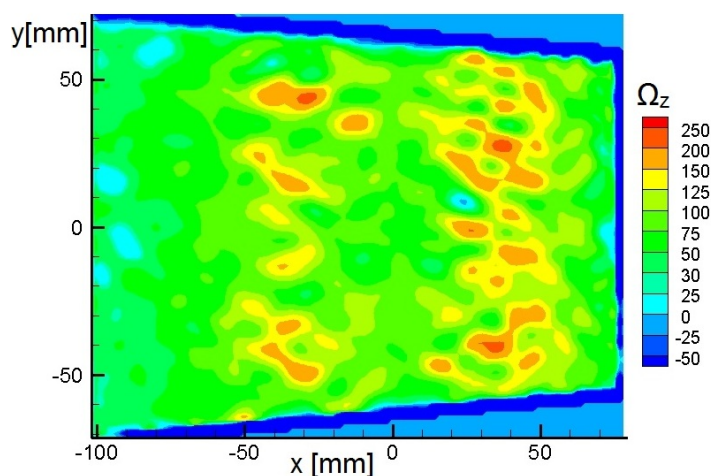


Figure 6. Average vorticity.

Vorticity could be easily related to the dissipativity. So, it can be concluded that intensive dissipation is generated in the shear layer bounded with maximum values of vorticity. As vorticity generation and its destruction are determined by the field of deformation of the vortex filaments and the viscosity influence, it is obvious that the obtained experimental results have great significance for the turbulence structure investigation. Namely, big whirls have the greatest energy, while the vorticity is in small-scale whirls. On the other hand, according to the cascade energy transfer, the dissipation process of turbulence kinetic energy happens in them.

An overview of the nine algorithms for vortex detection is provided in [19]. The “Lambda 2” method for vortex detection is proposed in paper [20]. It starts with the viewpoint that the pressure minimum is insufficient as a criterion for the vortex center detection. The velocity gradient \underline{J} ($\underline{J} \equiv \text{grad} \underline{c}$) tensor is decomposed in its symmetrical part \underline{S} and asymmetric part $\underline{\Omega}$, where they are defined as follows:

$$\underline{S} = \frac{1}{2}(\underline{J} + \underline{J}^T), \quad \underline{\Omega} = \frac{1}{2}(\underline{J} - \underline{J}^T) \tag{1}$$

The vortex is defined as the region of the connection, where the sum $\underline{S}^2 + \underline{\Omega}^2$ has two negative eigenvalues. This sum, real and symmetric, has only real eigenvalues. Let $\lambda_1 \geq \lambda_2 \geq \lambda_3$. If λ_2 has a negative value in one point, then this point belongs to the vortex core. There is a problem with this method if several vortex structures exist. It reveals numerous centers (Figure 7), which follow the main central vortex core region. So, in this case, the method used in the previous chapter with the total velocity minimum is more appropriate for the vortex dynamics study.

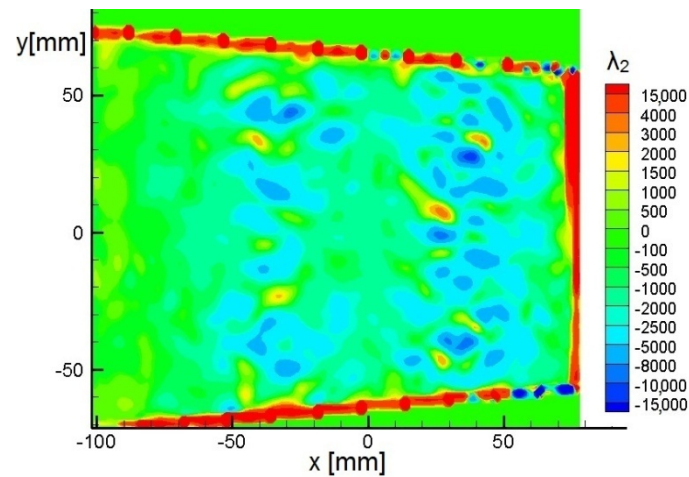


Figure 7. Distribution of λ_2 in the measuring cross-section.

5. Turbulence Statistics, Structure, and Discussions Using Invariant Theory

On the basis of the HSS PIV data, the Reynolds stresses are calculated, which are the input for the Lumley triangles. In Figure 8a, the normal Reynolds stress for the axial velocity $\overline{u^2}$ is presented, while in the Figure 8b, the shear stress \overline{uw} is presented. In this case, the normal stress has a minimum value, mainly in the vortex core zone, while this is not a case for the turbulent swirl flow, which is not axially restricted and has a maximum on the pipe axis. This is presented for the same axial fan type in [11,13–15]. The shear stress has higher values in the transient zone from the solid body to the free vortex, i.e., in the shear layer region.

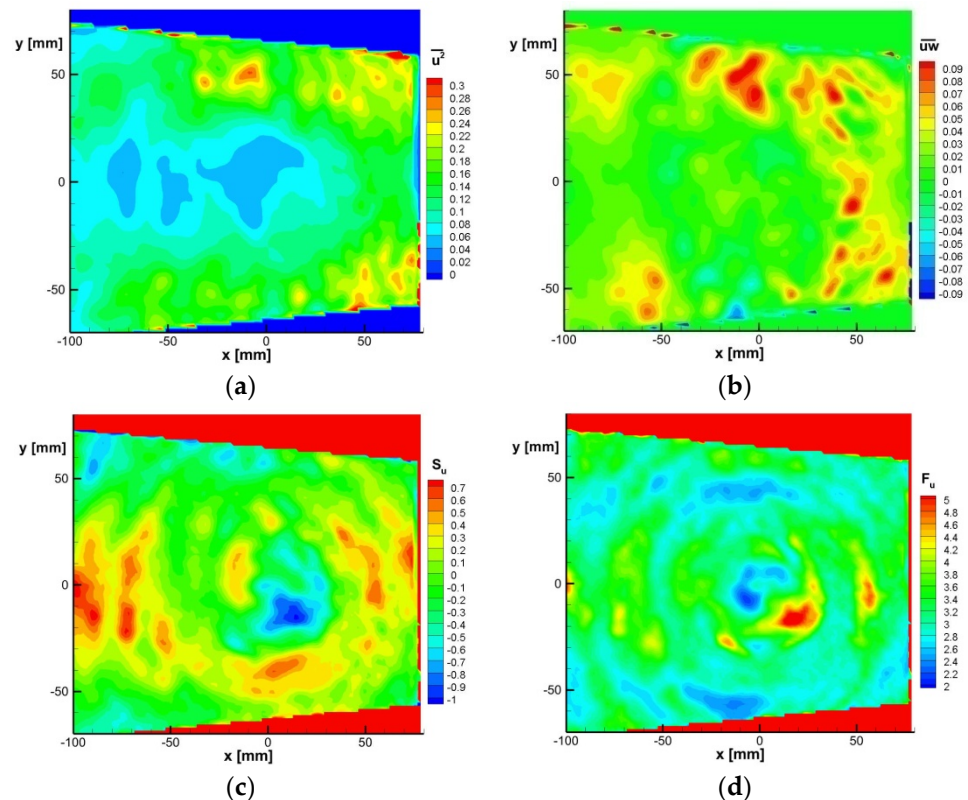


Figure 8. Reynolds stresses: (a) normal and (b) shear; statistical moments of higher order: (c) skewness factor and (d) flatness factor.

The statistical moments of the third order (skewness factor, S_u) and of the fourth order (flatness factor, F_u) of the axial fluctuating velocity are presented in Figure 8c,d, respectively. Their values differ from the values for normal, Gaussian distribution ($S_u = 0$ and $F_u = 3$), dominantly in the shear layer region, while there are also some extremes in the vortex core region. All these complex distributions emphasize a need for further analyses, as presented below.

The invariant theory of turbulence is applied for the anisotropy study. The underlying idea of this theory is a quantitative description of turbulence anisotropy. Lumley and Newman, in [21], introduced an anisotropy tensor $\underline{\underline{A}} = a_{ij}e_i e_j$ as a measure of turbulence:

$$\underline{\underline{A}} = -\left(\frac{1}{2\rho k}\underline{\underline{T}} + \frac{1}{3}\underline{\underline{I}}\right), \quad a_{ij} = \frac{1}{2k}\overline{u_i u_j} - \frac{1}{3}\delta_{ij}, \quad (2)$$

where $\underline{\underline{T}}$ is tensor of Reynolds stresses and k is turbulence kinetic energy. The mathematical formulation of three independent invariants and their application to vortex investigation is presented in [13–15,22,23] in the following way:

$$\begin{aligned} I_a &= 0, \\ II_a &= -\frac{1}{2}a_{ij}a_{ji}, \\ III_a &= \frac{1}{3}a_{ij}a_{ik}a_{jk}, \end{aligned} \quad (3)$$

where $a_{ij} = \frac{1}{2k}\overline{u_i u_j} - \frac{1}{3}\delta_{ij}$ and $k = \frac{1}{2}(\overline{u^2} + \overline{v^2} + \overline{w^2})$,

where k is turbulent kinetic energy, while δ_{ij} is Kronecker delta.

The determination of the second and the third invariants is possible using the HSS PIV experimental results, which provide all three of the velocity components. All of the possible states of turbulence anisotropy belong to the anisotropy invariant map-curvilinear triangle 012, i.e., the Lumley triangle (Figure 9), defined by Equation (3.4) in paper [22]. Figure 9 presents coordinates of the triangle vertices, of which 0 denotes the state of the three-component isotropic turbulence, point 1 corresponds to the boundary layer of the one-component isotropic turbulence, and 2 is two-component isotropic turbulence. Boundary 21 stands for the two-component turbulence, curve 01 denotes axisymmetric expansion, while curve 02 indicates axisymmetric contraction.

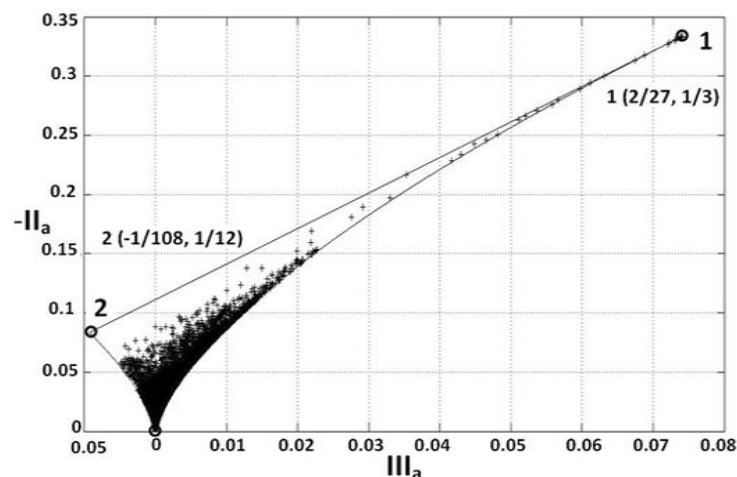


Figure 9. Anisotropy invariant map (Lumley triangle) for experimentally obtained results [14].

A set of values $(III_a, -II_a)$ for 11,210 points, obtained by 2771 image pairs in the time period of approximately 1.4 s, is presented in the Lumley triangle (Figure 9). It is obvious that all the values belong to the domain of the invariant map. The invariant map in Figure 9 includes various physically possible turbulence states in the measuring cross-section. The coordinates of the measurement point closest to the coordinate system origin ($x0y$) are

$x = -0.1818$ mm and $y = 0$ mm. For further calculation, $x = 0$ mm and $y = 0$ mm are adopted. In order to analyze the turbulence anisotropy, the directions of the x -axis and y -axis form a series of points where the values $(III_a, -II_a)$ are calculated. The smallest possible step is, due to the calibration file, approximately 1.45 mm in both directions, corresponding to the step 0.007 for $r = R$. A grid of measurement and calculation points for invariant maps, along radii defined by angles $\varphi = 0^\circ; 90^\circ; 180^\circ; \text{ and } 270^\circ$, is formed and presented in Table 1.

Table 1. Numeric grid for invariant maps.

φ [°]	0	90	180	270
Def. of the rad. dir.	$x > 0$	$y > 0$	$x < 0$	$y < 0$
Num. of calc. points	53	44	70	44

Obviously, there are approximately 30% more points in the x -axis direction.

Lumley triangles are presented individually for measuring points along the axis $x > 0$, $y > 0$, $x < 0$, and $y < 0$. It is evident that the invariant values $(III_a, -II_a)$ in the points along the x -axis are mainly distributed in the right part of the invariant map and along the line 01, which characterizes axisymmetric expansion (Figure 10a,b).

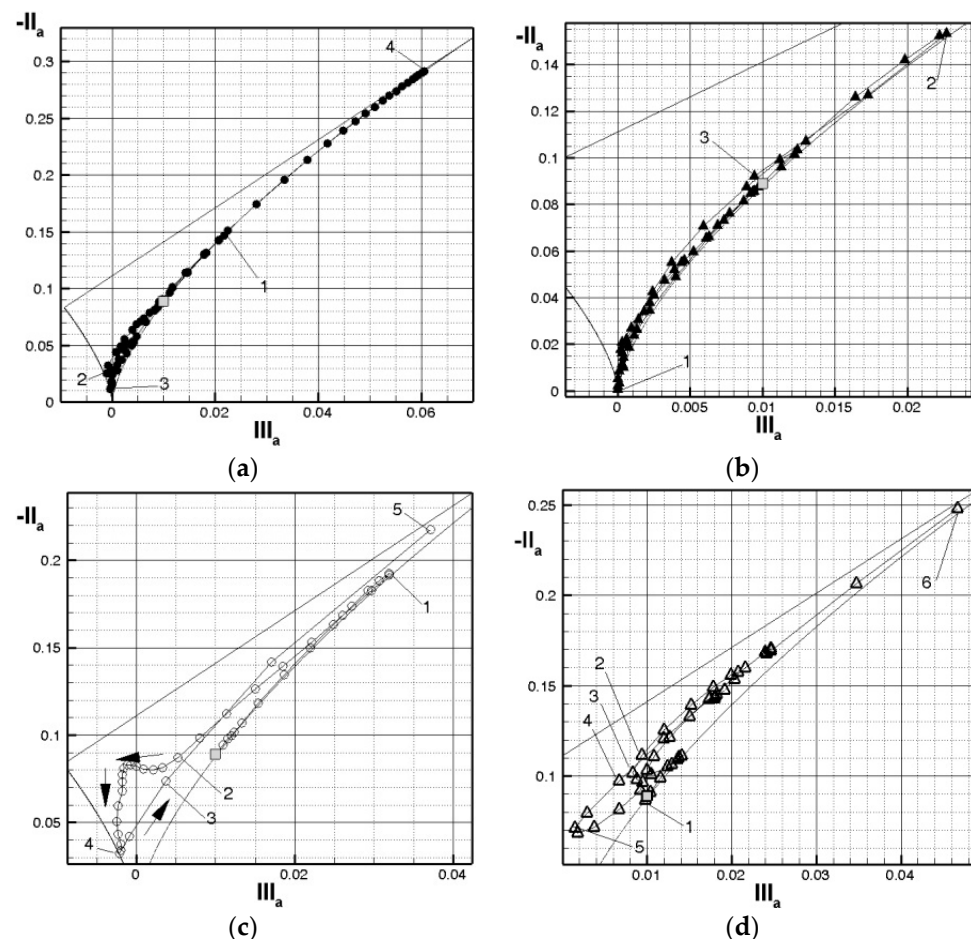


Figure 10. Trajectories of the anisotropy invariants for four radii defined by the angle φ : (a) 180° , (b) 0° , (c) 270° , and (d) 90° .

The density of the points is the greatest in the lower part of the invariant map, in the domain between curves 20 and 01 in the neighborhood of point 0 for points along the x -axis, which defines the three-component isotropic turbulence. The distributions of the invariants of the anisotropy tensor of turbulent stresses are, however, of a different

character for a set of points along the y -axis. Namely, in Figure 10c,d it is visible that the points are distributed in the middle and upper domain of the invariant map. The values of the pairs of anisotropy invariants ($III_a, -II_a$) for points along the y -axis are higher to the center of the Lumley triangle, and their distribution becomes more complex in the lower part of the map.

On the basis of previous analysis, it can be concluded that turbulence flow, analyzed in this paper, is characterized by distinguished anisotropy, as well as that anisotropy of various kinds is present in various flow regions in the pipe cross-section. A special point, which is on the pipe axis, is marked by the square gray symbol. The region of the pipe axis in Figure 10a is characterized by the values of the pair of invariants that are on the right curve of axisymmetric turbulence. From here, a small wavering of the trajectory in the direction of the left curve of axisymmetric turbulence exists, where a significant motion of the pair of invariants occurs in the direction of strong anisotropy to point 1, which denotes the position in pipe $r/R = 0.057$ (Figure 10a). It is approximately on the first third of the right curve of axisymmetric turbulence. Afterwards, the trajectory stops in close vicinity of the left curve of axisymmetric turbulence in the position $r/R = 0.155$ (point 2, Figure 10a). This is still the vortex core region. It can be noticed that in a very small area, especially in the vortex core region, significant changes of turbulence characteristics take place. The pair of invariants shows a tendency of further motion in the central area of the Lumley triangle.

In point $r/R = 0.281$ (point 3, Figure 10a), which is in the main flow region, the pair of invariants approaches very close to the region of three-component isotropic turbulence. From here, the trajectory is spreading itself very close to the right curve, which characterizes axisymmetric turbulence, and ends in almost the most extreme position in the region of total anisotropy in point 4, which denotes position $r/R = 0.484$ (Figure 10a). In the region $\varphi = 0^\circ$ (Figure 10b), the trajectory has a similar character, but another point occurs, which is even closer to the three-component isotropic turbulence in the position $r/R = 0.097$ (point 1, Figure 10b). In the position $r/R = 0.356$ (point 2, Figure 10b), the trajectory ends with its maximum deviation in the map right side. It ends in the position $r/R = 0.37$ (point 3, Figure 10b).

In the direction shown in Figure 10c, the dominant positioning of the trajectory is noticeable close to the right curve of the axisymmetric turbulence, in the direction of total anisotropy, all the way to the position $r/R = 0.091$ (point 1, Figure 10c). The pair of invariants, using the shortest path, moves from here towards the central area of the Lumley triangle, where there is a significant number of points in this area $r/R = 0.154 \div 0.287$ (points 2 and 3 respectively, Figure 10c). In the position $r/R = 0.266$ (point 4, Figure 10c), the trajectory reaches its final left position, from where, again, using the shortest way, it reaches its final right position in point $r/R = 0.301$ (point 5, Figure 10c). So, the distinguished changes of turbulence character in such a small area indicate the very complex structure of the studied turbulent flow.

Along the direction $\varphi = 90^\circ$ (Figure 10d), similar regimes in the sense of turbulence characteristics occur, where the main zone of change of movement is in the area between axisymmetric and two-component turbulence for the interval $r/R = 0.007 \div 0.175$ (points 1 and 2, respectively, Figure 10d). The central region of the Lumley triangle is reached in the interval $r/R = 0.182 \div 0.245$ (points 3 and 4, respectively, Figure 10d), where in the position $r/R = 0.231$ (point 5, Figure 10d) the trajectory approaches very close to the left curve of the axisymmetric turbulence. From this position, the trajectory is heading to the area of the second third of the invariant map, where it ends in the position $r/R = 0.308$ (point 6, Figure 10d).

6. Conclusions

Fans, as well as pumps, are the most frequently used turbomachines; moreover, electro motors, and machines in general, still challenge science. The presented research of the turbulent swirl flow behind the axial impeller in the pipe has numerous technical applications, and it is significantly correlated with the system energy efficiency.

The main achievements of the paper, which presents the new approach in the analysis of the turbulent swirl flow dynamics and structure in the pipe behind the axial fan impeller, are:

- The application of the turbulence statistics (the statistical moments of a higher order) in the turbulent swirl flow study on the basis of the HSS PIV data. The calculated Reynolds stresses are input for the second main point of these paper-invariant maps;
- The high-speed stereo PIV data are implemented in the invariant maps for the faster study of the turbulence anisotropy;
- The vortex dynamics investigation by the use of the total velocity minima criterion;
- The first presented contribution is usually implemented in a discussion on the basis of the experimental results obtained by the point-wise measurement methods, such as HWA or LDV. However, in this paper it is shown how the distribution of skewness and flatness factors in a wide area, captured at the same time, could provide better insight into the position of the shear layer region.

The second main contribution reveals the possibility to study turbulence states in a widely known anisotropy map, which could provide a quick overview of the studied flow. Effectively, up to now, this map has, again, usually been used only in cases of point-wise measurement methods [24]. HSS PIV data are implemented in the invariant maps in the case of turbomachinery for the first time in the papers. The presented idea in this paper is successfully implemented and published in the papers [22,23], and this was the case of the wing tip vortex formed behind the NASA CRM wing. So, it is shown here that it could be equally successful in application in turbomachinery.

The developed observation of the vortex dynamics, which is the third main achievement of this paper, enables users to understand how the energy is consumed. In fact, more unique points or a wider area, where total velocity minima occur, results in more intensive energy decay. In other words, the more intensive dynamics, the greater the losses are. The vortex dynamics are analyzed using the criterion based on the statistical-numerical determination of the set of chaotic positions and trajectories of the total velocity minima positions. An investigation of the vortex behavior, and a comprehensive statistical analysis of this phenomenon, is presented.

A number of open questions are raised, and they require further research to be answered. Further analysis would be focused on the detailed study of coherent vortex structures, the vortex dynamics, and the strong intermittency in the swirl turbulence. Further physical analysis of the experimental results could be performed to determine the substantial influence of the swirl on turbulence anisotropy. Anisotropy leads to a change of turbulent dissipation and turbulent kinetic energy, which changes the energy characteristics of the flow system. This presents the most important questions in the theoretical study of turbulence in a rotating fluid, and in the modeling of non-local turbulent transfer in non-isotropic turbulent swirl flow generated by axial fan impellers.

Author Contributions: Conceptualization, D.S.Č.; methodology, D.S.Č.; software, D.S.Č. and N.Z.J.; validation, D.S.Č.; formal analysis, D.S.Č. and N.Z.J.; investigation, D.S.Č. and N.Z.J.; resources, D.S.Č. and N.Z.J.; data curation, N.Z.J.; writing—original draft preparation, D.S.Č.; writing—review and editing, D.S.Č.; visualization, D.S.Č. and N.Z.J.; supervision, D.S.Č.; project administration, D.S.Č. and N.Z.J.; funding acquisition, D.S.Č. All authors have read and agreed to the published version of the manuscript.

Funding: This research was funded by the Ministry of Education, Science, and Technological Development, Republic of Serbia, grant number 451-03-68/2022-14/200105, subproject TR35046 and Steinbeis University Berlin, Institute Corporate Responsibility Management, which is gratefully acknowledged.

Acknowledgments: In memory of Zoran D. Protić (1922–2010), University of Belgrade, Faculty of Mechanical Engineering. He was an outstanding professor in Turbomachinery at our University. He initiated the first experimental investigations of the turbulent swirl flow at our University and designed the axial fan used in this research.

Conflicts of Interest: The authors declare no conflict of interest.

References

1. Kim, Y.-I.; Lee, S.-Y.; Lee, K.-Y.; Yang, S.-H.; Choi, Y.-S. Numerical Investigation of Performance and Flow Characteristics of a Tunnel Ventilation Axial Fan with Thickness Profile Treatments of NACA Airfoil. *Energies* **2020**, *13*, 5831. [CrossRef]
2. Ye, X.; Fan, F.; Zhang, R.; Li, C. Prediction of Performance of a Variable-Pitch Axial Fan with Forward-Skewed Blades. *Energies* **2019**, *12*, 2353. [CrossRef]
3. Zhang, L.; Zhang, L.; Zhang, Q.; Jiang, K.; Tie, Y.; Wang, S. Effects of the Second-Stage of Rotor with Single Abnormal Blade Angle on Rotating Stall of a Two-Stage Variable Pitch Axial Fan. *Energies* **2018**, *11*, 3293. [CrossRef]
4. Huang, W.; Chen, L.; Yang, L.; Du, X. Energy-Saving Strategies of Axial Flow Fans for Direct Dry Cooling System. *Energies* **2021**, *14*, 3176. [CrossRef]
5. Benišek, M.; Protić, Z. Investigation of the Lost Flow Energy for Swirling Flow in Long Lined Circular Pipes. In Proceedings of the 15th Yugoslav Congress of Theoretical and Applied Mechanics, Belgrade, Yugoslavia, 1–5 June 1981; Volume B, pp. 269–276.
6. Cory, W.T.W. *Fans and Ventilation: A Practical Guide*; Elsevier: Amsterdam, The Netherlands, 2005; p. 424.
7. Benišek, M.; Čantrak, S.; Nedeljković, M. Theoretical and Experimental Investigation of the Turbulent Swirling Flow Characteristics in Circular Pipes. *ZAMM* **1988**, *68*, T280–T282.
8. Benišek, M.H.; Lečić, M.R.; Čantrak, Đ.S.; Ilić, D.B. The School of the Turbulent Swirling Flow at the Faculty of Mechanical Engineering University of Belgrade. *Thermal Science* **2017**, *21* (Suppl. S3), S899–S911. [CrossRef]
9. Eck, B. *Ventilatoren—Entwurf und Betrieb der Radial-, Axial- und Querstromventilatoren*, 6th ed.; Springer: Berlin/Heidelberg, Germany, 2003; p. 595.
10. Protić, Z.D.; Nedeljković, M.S.; Čantrak, Đ.S.; Janković, N.Z. Novel Methods for Axial Fan Impeller Geometry Analysis and Experimental Investigations of the Generated Swirl Turbulent Flow. *Therm. Sci.* **2010**, *14*, S125–S139. [CrossRef]
11. Čantrak, Đ.S.; Čolić Damjanović, V.M.Z.; Janković, N.Z. Study of the Turbulent Swirl Flow in the Pipe behind the Axial Fan Impeller. *Mech. Ind.* **2016**, *17*, 412. [CrossRef]
12. Mattern, P.; Sieber, S.; Čantrak, Đ.; Fröhlig, F.; Caglar, S.; Gabi, M. Investigations on the Swirl Flow Caused by an Axial Fan: A Contribution to the Revision of ISO 5801. In Proceedings of the Fan 2012, International Conference on Fan Noise, Technology and Numerical Methods, Senlis, France, 18–20 April 2012. 11p.
13. Čantrak, Đ.S.; Janković, N.Z.; Lečić, M.R. Laser Insight into the Turbulent Swirl Flow behind the Axial Flow Fan. In Proceedings of the ASME Turbo Expo 2014: Turbine Technical Conference and Exposition, GT 2014, Technical track: Fans and Blowers, ASME TURBO EXPO 2014, Düsseldorf, Germany, 16–20 June 2014; p. V01AT10A024.
14. Čantrak, Đ.S. Analysis of the Vortex Core and Turbulence Structure behind Axial Fans in a Straight Pipe using PIV, LDA and HWA Methods. Ph.D. Thesis, University of Belgrade, Faculty of Mechanical Engineering, Belgrade, Serbia, 30 July 2012. Available online: <http://doiserbia.nb.rs/phd/fulltext/BG20120730CANTRAK.pdf> (accessed on 1 July 2022).
15. Čantrak, Đ.S. *Investigation of the Turbulent Rankine Vortex in the Pipe behind the Axial Fan Impeller Using Optical (PIV and LDA) Measurement Methods and Visualization*; Military Technical Institute: Belgrade, Serbia, 2022; p. 163.
16. Javadi, H.; Nilsson, S. LES and DES of Strongly Swirling Turbulent Flow through a Suddenly Expanding Circular Pipe. *Comput. Fluids* **2015**, *107*, 301–313. [CrossRef]
17. Sciacchitano, A. Uncertainty Quantification in Particle Image Velocimetry. *Meas. Sci. Technol.* **2019**, *30*, 092001. [CrossRef]
18. Mattern, P.; Sieber, S.; Dues, M.; Caglar, S.; Gabi, M. Simultaneous High Speed Stereo PIV and LDA Measurements in the Highly Transient Vortical Wake of an Axial Fan. In Proceedings of the 16th Int. Symp. on Applications of Laser Techniques to Fluid Mechanics, Lisbon, Portugal, 9–12 July 2012. 11p.
19. Jiang, M.; Machiraju, R.; Thompson, D. *Detection and Visualization of Vortices*, 14. Chapter in the Book *The Visualization Handbook*; Hansen, C.D., Johnson, C.R., Eds.; Elsevier Butterworth-Heinemann: Burlington, MA, USA, 2005.
20. Jeong, J.; Hussain, F. On the Identification of a Vortex. *J. Fluid Mech.* **1995**, *285*, 69–94. [CrossRef]
21. Lumley, J.L.; Newman, G. The Return to Isotropy of Homogenous Turbulence. *J. Fluid Mech.* **1977**, *82*, 161–168. [CrossRef]
22. Čantrak, Đ.S.; Kushner, L.K.; Heineck, J.T. Time-resolved Stereo PIV Investigation of the NASA Common Research Model in the NASA Ames Fluid Mechanics Laboratory 32- by 48-in Indraft Wind Tunnel. In *CTR Research Publications, Center for Turbulence Research, Annual Research Briefs*; Center for Turbulence Research: Stanford, CA, USA, 2014; pp. 179–191.
23. Čantrak, Đ.S.; Heineck, J.T.; Kushner, L.K.; Janković, N.Z. Turbulence Investigation of the NASA Common Research Model Wing Tip Vortex. *Therm. Sci.* **2017**, *21* (Suppl. S3), S851–S862. [CrossRef]
24. Jovanović, J. *The Statistical Dynamics of Turbulence*; Springer: Berlin/Heidelberg, Germany, 2004; p. 141.